The role of singlet oxygen, superoxide, hydroxide, and hydrogen peroxide in the photoelectrochemical response of phenols at a supported highly fluorinated zinc phthalocyanine

The Role of Singlet Oxygen, Superoxide, Hydroxide and Hydrogen Peroxide in the Photoelectrochemical Response of Phenols at a Supported Highly Fluorinated Zinc Phthalocyanine

Liselotte Neven,[a,b] Hanan Barich,[a,b] Marius Pelmuş,[c] Sergiu M. Gorun,[c] and Karolien De Wael*[a,b]

[a] L. Neven, H. Barich, K. De Wael
A-Sense Lab
Department of Bioscience Engineering
University of Antwerp
Groenenborgerlaan 171, 2020 Antwerp, Belgium
E-mail: karolien.dewael@uantwerpen.be

[b] L. Neven, H. Barich, K. De Wael
NANOlab Center of Excellence
University of Antwerp
Groenenborgerlaan 171, 2020 Antwerp, Belgium

[c] M. Pelmuş, S. M. Gorun
Department of Chemistry and Biochemistry and the Center for Functional Materials
Seton Hall University
400 South Orange Ave, New Jersey, 07079, USA

Supporting information for this article is given via a link at the end of the document.

Abstract: Photoelectrochemical (PEC) sensing of phenolic compounds using singlet oxygen ($^1O_2$)-generating photocatalysts has emerged as a powerful detection tool. However, it is currently not known how experimental parameters, such as pH and applied potential, influence the generation of reactive oxygen species (ROS) and their photocurrents. In this article, the PEC response was studied over the 6 to 10 pH range using a rotating (ring) disk (R(R)DE) set-up in combination with quenchers, to identify the ROS formed upon illumination of a supported photosensitizer, F_{64}PcZn. The photocurrents magnitude depended on the applied potential and the pH of the buffer solution. The anodic responses were caused by the oxidation of $O_2^{\bullet-}$, generated due to the quenching of $^1O_2$ with $^{\bullet}OH$ and the reaction of $^3O_2$ with [F_{64}Pc(3-)Zn]. The cathodic responses were assigned to the reduction of $^1O_2$ and $O_2^{\bullet-}$, yielding H_2O_2. These insights may benefit $^1O_2$ – based PEC sensing applications.

1. Introduction

Singlet delta oxygen ($^1O_2$), the excited form of O_2, is one of the main reactive oxygen species (ROS).[1] It is a better oxidant than O_2 as it has a standard reduction potential (E^0) vs SHE of 0.65 V, compared to -0.33 V for O_2.[1c] This has led to the use of $^1O_2$ as the basis of a new photoelectrochemical (PEC) strategy for the detection of phenolic compounds, which are recognized as priority pollutants.[2] Briefly, the aerobically produced $^1O_2$ by a photosensitizer (type II PS) placed on a PEC sensor, oxidizes phenolic compounds, followed by their reduction at the electrode surface to generate a signal and a redox cycle. A highly sensitive sensor was thus developed, with detection limits (LOD) for antibiotics and phenols in the nmol L^{-1} range.[2a, 2b] However, how experimental conditions, such as pH and applied potential, influence the generation of ROS and their contribution to the observed photocurrents is not understood. Specifically, why the oxidative contribution to the reductive photocurrent increases with the alkalinity of the buffer solution was unclear. This pH effect was observed during the optimization of the PEC detection for antibiotics.[2a] Thus, a detailed analysis of the ROS contributions to the photocurrent responses is necessary for the understanding of the PEC sensor behavior, as well as to implement and optimize the $^1O_2$-driven oxidation of the phenols.

The majority of ROS derived from the (electrochemical) reduction of $^1O_2$ and O_2, are $O_2^{\bullet-}$, H_2O_2 and $^{\bullet}OH$.[1, 3] In contrast to $^1O_2$, the species $O_2^{\bullet-}$ (pk_a = 4.8), H_2O_2 (pk_a = 11.7), and $^{\bullet}OH$ (pk_a = 11.9) exhibit acid-base equilibria rendering their oxidation (rates) pH-dependent.[1a, 4] For instance, $O_2^{\bullet-}$ which is a mild oxidant[4-5] becomes a very strong oxidant upon protonation due to the removal of the negative charge, which repels electron-rich centers.[1c, 6] Furthermore, the concentration of protons together with the applied electrochemical potential can also influence the occurrence of various electrochemical reactions.[7]

ROS detection methods usually involve a reaction with a probe, for example, 5,5-dimethyl-1-pyrroline-N-oxide (DMPO), detected via EPR spectroscopy, or luminol and Amplex® Red detected by chemiluminescence and fluorescence spectroscopy, respectively, or nitro blue tetrazolium (NBT) and UV-Vis detection.[1a, 8] While useful for the detection of ROS, these methods, in the case of a PEC sensor, may not be applicable since the initially PS-produced ROS undergo reduction or oxidation at the electrode, leading to a new set of ROS. Thus, these ROS produced during electrochemical measurements must be identified, for example, by using quenchers such as NaN_3, catalase, or superoxide dismutase (SOD), as demonstrated by Kornienko *et al.*[3] They used a rotating disk electrode (RDE) and rotating ring disk electrode (RRDE) set-up for their studies of Photosystem II. R(R)DE detection advantageously is based on the constant diffusion of reactants towards the electrode surface and thus allows the efficient identification of the ROS upon the addition of quenchers.

We report here the identification using R(R)DE of ROS (which include $^1O_2$, $O_2^{\bullet-}$ and H_2O_2), aggressive species, without interference from their potential destructive reactivity with the PS that produces them.[9] The robustness of the PS is critically important not only for ensuring a viable PEC sensor technique that could be used repeatedly without loss of performance, but also for ensuring that the species produced are not consumed by side-reactions with the photocatalyst, instead of oxidizing the

analyte. The chosen PS, the perfluorinated phthalocyanine zinc complex, $F_{64}Pc(2\text{-})Zn$, meets the above conditions by its resistance to nucleophilic, electrophilic and radical degradation pathways.[9] Moreover, the photocatalyst should exhibit reversible redox properties, in the case of the closed-shell $F_{64}Pc(2\text{-})Zn$, centered entirely on the HOMO-LUMO of the fluoro-organic macrocycle: $F_{64}Pc(2\text{-})Zn \leftrightarrow F_{64}Pc(3\text{-})Zn$. Notably, $F_{64}Pc(3\text{-})Zn$ is actually the stable radical anion derived from $F_{64}Pc(2\text{-})Zn$, namely $[F_{64}Pc(2\text{-})Zn]^{\bullet-}$ and thus its reaction with the $^3O_2$ diradical is likely to advantageously be diffusion controlled.

Therefore, the different ROS generated in this PEC sensor will be identified in this research in order to elucidate the PEC sensing mechanism. This elucidation relies upon (i) the understanding of the redox chemistry $F_{64}PcZn$, (ii) its ability to produce $^1O_2$, as evidenced by HPLC-diode array detector (HPLC-DAD) measurements, and (iii) the detection of $^1O_2$, $O_2^{\bullet-}$ and H_2O_2 using quenchers and RDE and RRDE measurements. These ROS will be studied in the pH range of 6 – 10. The cathodic responses will be studied at reductive potentials as this is the potential region in which the sensor operates. However, the increasing of buffer pH, which is beneficial for enlarging the oxidation rate of phenols with $^1O_2$, elevates the anodic responses at a specific potential.[2a] As a result, the anodic responses will also be studied to understand the impact of the pH on the sensing mechanism. This will be achieved by assessing the responses at oxidative potentials to exclusively exhibit to the PEC mechanism for generating anodic responses. As a result, the PEC sensing mechanism will be studied in the potential region between 0.25 V to -0.25 V vs SCE. Insights in the role of ROS under various experimental conditions are crucial for the selection of optimum experimental parameters for PEC detection.

2. Results and Discussion

2.1 Electrochemical behavior of $F_{64}PcZn$

The structure of the photosensitizer $F_{64}PcZn$ is shown in Figure S1. Axial ligands, including organic solvents and H_2O may bind to the Zn^{2+} center, whose hydrophilicity is exacerbated by the fluorinated ligands. The metal center may also serve as a surface anchoring point. Both axial binding and surface oxygen coordination are expected to alter somewhat the energies of the frontier orbitals, and thus redox potentials, but not the HOMO-LUMO gap, thus leaving the absorption of energy centered in the red region of the electromagnetic spectrum largely unchanged.[10] The aim is to understand if $F_{64}PcZn$ can be reduced or oxidized in the studied potential region (0.25 V to -0.25 V vs SCE) as this can impact the ROS generation in the PEC sensor. Solution studies represent the first step in gaining insights into the redox behavior of the PS, including reactions induced by it, which might occur during PEC measurements at a specific applied potential.

The cyclic voltammograms (CV) of $F_{64}PcZn$ in acetone, dimethylformamide (DMF) and acetonitrile using a Pt mesh are shown in Figure S3, along with the corresponding differential pulse voltammetric (DPV) data and spectroelectrochemistry data. In all solvents, in the absence of O_2[11] the reductions are favorable, consistent with previous results.[12] The one-electron reduction process $F_{64}Pc(2\text{-})Zn \leftrightarrow F_{64}Pc(3\text{-})Zn$ when -0.7 V vs Ag/AgCl (-0.74 V vs SCE) is applied, is not only clean, consistent with the literature,[12] as indicated by the isosbestic points, but also fully reversible at open circuit potential, Figure S3 (D-G). The spontaneous re-oxidation process is consistent with the long-term viability of electron transfer-based devices using $F_{64}PcZn$ and confirms the advantageous choice of the PS. In the case of PEC, the study of the electrochemical behavior of $F_{64}PcZn$, immobilized on a support, was extended to aqueous buffers.

The redox features of supported $F_{64}PcZn$ in pH 7 phosphate buffer were determined via CV measurements. A stock solution of $F_{64}PcZn$ in ethanol (EtOH) was diluted with Milli Q water to allow efficient dropcasting on the working electrode (WE) of the screen-printed electrode (SPE). The droplets were left to dry overnight. Earlier characterization of $F_{64}PcZn$ in DMF solution[12] revealed reduction and oxidation signals in the O_2 reduction region. Before the CV measurements, the solution was therefore purged with Ar for 15 minutes, to minimize the contribution of the O_2 reduction peak (Figure S4) and improve the visibility of the redox peaks (Figure 1). Two reduction peaks, -0.47 V vs SCE (R1) and -0.76 V vs SCE (R2), and only one broad oxidation peak, -0.39 V vs SCE (O1), were observed when $F_{64}PcZn$ was immobilized on the WE surface (Figure 1, red). These peaks, as mentioned above, were attributed to the Pc rings reductions and re-oxidation that regenerate the neutral species.[12] No peaks were observed when only a mixture of EtOH and H_2O was deposited on the surface of the electrode; only a spike originating from the Ag of the RE on the WE surface was obtained (Figure 1, black).[13] The observed reduction peaks were slightly shifted towards oxidative potentials in comparison with the PS solubilized in DMF (-0.43 V and -0.92 V vs Ag/AgCl)[12] due to the deposition of the PS on the WE and the solvent-dependent variation of the redox potential. When the CV was recorded from the $F_{64}PcZn|TiO_2$-coated WE, these redox features could not be observed as they were masked by the large contribution from TiO_2 (Figure S5). So, in the studied potential region between 0.25 to -0.25 V vs SCE, it is expected that $F_{64}PcZn$ retains its photoactivity as it is not electrochemically reduced by the application of a specific potential in that region.

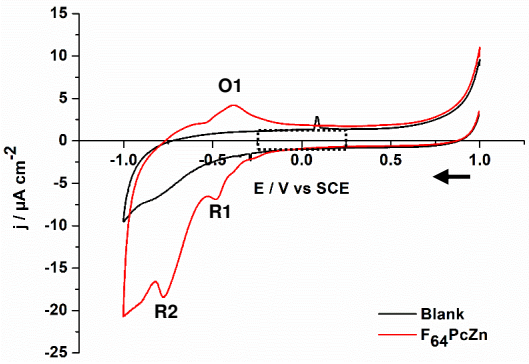

Figure 1. CV of 0.5 nmol $F_{64}PcZn$ (red line), deposited from an EtOH-H_2O mixture, recorded in pH 7 phosphate buffer in Ar atmosphere. The blank trace originates from the EtOH-H_2O mixture, without PS (black line) deposited on the SPE. The scan rate was 0.05 V s^{-1}. The arrow indicates the scan direction. Box indicates the operational range for PEC sensing.

2.2 The pH-effect on photocurrents

The photocurrents generated by the illuminated $F_{64}PcZn|TiO_2$-coated WE were evaluated using a three-electrode RDE set-up. In general, the rotation speed does not influence the

obtained responses significantly.[3] As a result, a rotation speed of 500 rpm was chosen to allow a sufficient flow of reactants towards the surface and to ensure the stability of the dropcasted coating during these measurements. The $F_{64}PcZn|TiO_2$-coated RDE surface was subjected to chopped red laser illumination to determine the baseline current and photocurrent response in a single amperometric measurement. The applied potential ranged from 0.25 V to -0.25 V vs SCE (Figure 2). In that potential region, $F_{64}PcZn$ cannot be electrochemically reduced since its first reduction potential is more negative (Figure 1).

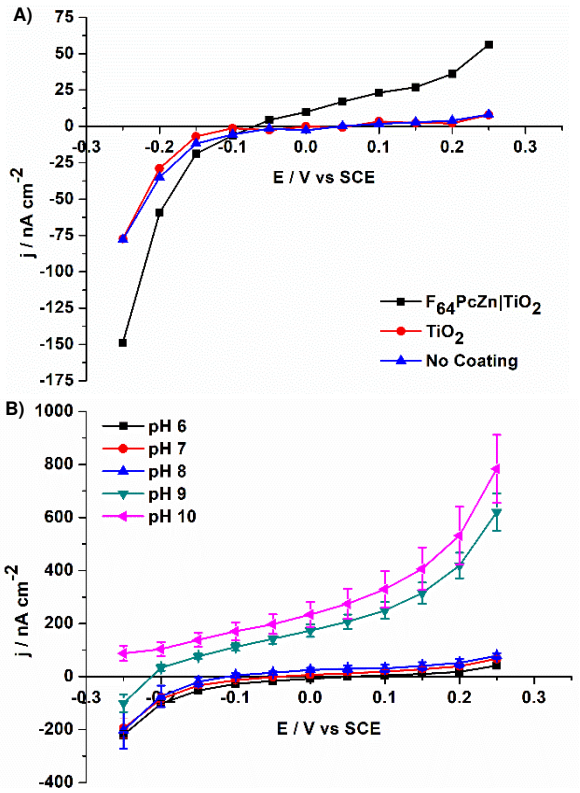

Figure 2. RDE photocurrent responses obtained (A) in pH 7 phosphate buffer with $F_{64}PcZn|TiO_2$-coated RDE (black, square), TiO_2 coating (red, dot) and no coating (blue, triangle) (N = 1). (B) RDE measurements in pH 6, 7, 8, 9 and 10 with $F_{64}PcZn|TiO_2$ as coating. Error bars denote the standard deviation of data obtained from 4 electrodes (N = 4). The RDE was illuminated by a 655 nm diode laser. All measurements were conducted in aerobic conditions.

A potential-dependent photoresponse was observed at pH 7 (Figure 2.A). The obtained responses showed a region of anodic photocurrents, from 0.25 V to -0.05 V vs SCE, and cathodic photocurrents from -0.1 V to -0.25 V vs SCE. In contrast, the photosignals caused by the bare RDE and TiO_2-coated RDE were negligible, indicating that TiO_2, as expected, is photoinactive at the used laser wavelength. Only at more negative potentials, e.g., from -0.15 V vs SCE on, an increasing reductive response was observed for the bare RDE and TiO_2-coated RDE. This was likely the result of the O_2 reduction[11] at the RDE, which drastically influenced the baseline current (Figure S6).

Interestingly, the anodic and cathodic photoresponses of $F_{64}PcZn|TiO_2$ were dependent on the pH of the buffer solution, as illustrated in Figure 2.B. The increase in pH elevated, in general, the oxidative contribution to the overall observed photoresponse. The potential at which reductive photoresponses were observed shifted towards more reductive potentials with higher pH levels, e.g. from 0.05 V vs SCE for pH 6 to -0.25 V vs SCE for pH 9. As a result, the reductive responses for pH 9 were smaller at -0.25 V vs SCE compared to the more acidic pH levels. This latter observation suggests the involvement of H^+ ions in the electrochemical reduction reactions. At pH 10, no reductive photocurrents were observed between 0.25 V to -0.25 V vs SCE. The photoresponses of bare RDE and TiO_2-coated RDE in borate buffer remained negligible (Figure S7).

Thus, the photocurrent responses clearly depend on the pH of the solution; the ^-OH and H^+ ions must be involved for the anodic and cathodic responses, respectively.

2.3 Cathodic photocurrents

In this part, the aim is to understand the mechanistic pathways of the reduction reactions at the PEC sensors and the involving ROS. Therefore, reductive potentials were applied, i.e. -0.15 V, -0.2 V or -0.25 V vs SCE, to induce these reactions in combination with pH 7 and pH 9 to assess the role of H^+ ions.

The role of O_2

Before the identification of the ROS involved in the photoresponses, it is important to understand the role of O_2 itself in these responses. To completely remove the O_2 in this set-up, a 3 hours purge with Ar was needed. The RDE photoresponses almost completely disappeared regardless of the pH (Figure 3). The photocurrent at pH 7 was five times smaller in an Ar atmosphere compared to that observed in an O_2 one (Figure 3.A). To obtain cathodic responses at pH 9, a much more reductive potential had to be applied, -0.25 V vs SCE. Also, at this pH, a large decrease in the cathodic signal was noted (Figure 3.B) in Ar atmosphere, an observation that corroborates that the cathodic photocurrents are completely dependent on the presence of O_2 for both pH levels and that the mechanisms behind these reductive responses are similar for both pHs.

Generation of $^1O_2$

$F_{64}PcZn$ is a known PS type II. Its quantum yield for generating $^1O_2$ has been determined in various solvents, for example methanol (MeOH) and acetone.[2b, 14] This PS, deposited on TiO_2, has been shown to produce $^1O_2$ while the material was embedded in polymers.[15]

To verify that $^1O_2$ is generated by $F_{64}PcZn|TiO_2$ in buffer solution, a $^1O_2$ quencher was employed. When choosing a quencher, it is imperative to understand if the alteration of the photocurrents is the result of a minimized reduction of $^1O_2$ at the electrode surface[3], due to the quenching reaction of $^1O_2$, or the result of an electrochemical reaction of the formed products after quenching.

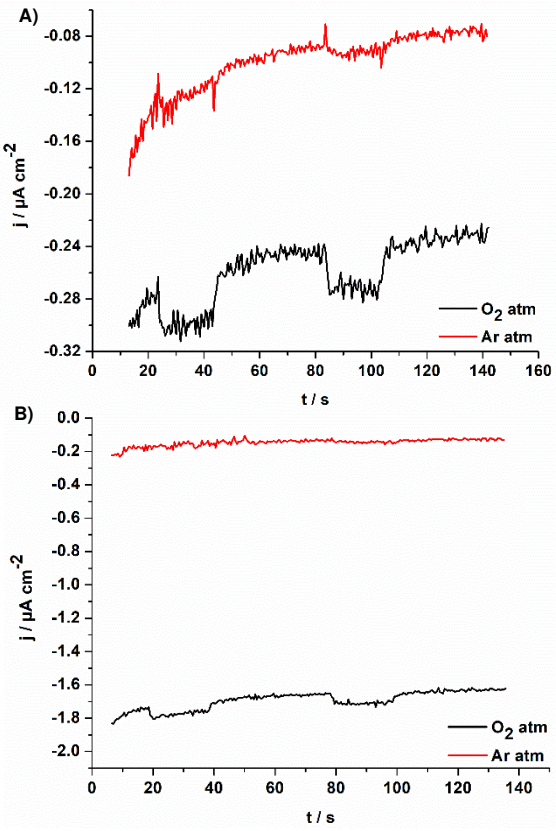

Figure 3. RDE photocurrents measured in O_2 (black) and Ar atmosphere (red) in (A) pH 7 phosphate buffer at -0.15 V vs SCE and (B) pH 9 borate buffer at -0.25 V vs SCE. RDE coating was $F_{64}PcZn|TiO_2$ and the RDE was illuminated by a 655 nm laser (switched on and off alternatingly).

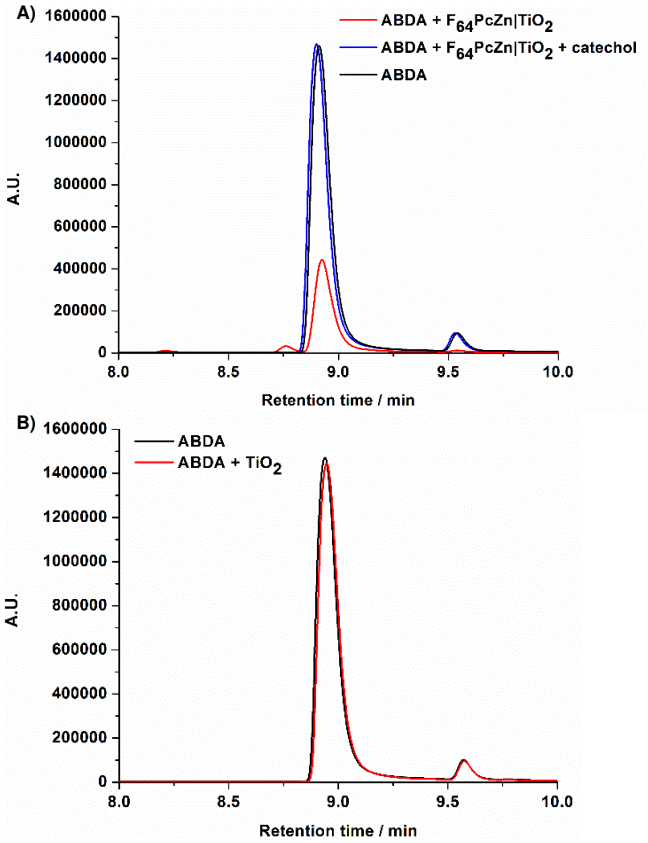

Figure 4. HPLC-DAD chromatograms recorded of a solution of 400 µmol L^{-1} ABDA (black) in overlay with (A) chromatograms of the ABDA-$F_{64}PcZn|TiO_2$ (red) and ABDA-$F_{64}PcZn|TiO_2$-catechol (blue) illuminated mixtures. The added concentration of catechol was 50 mmol L^{-1}. (B) Chromatogram of ABDA-TiO_2 illuminated mixture in overlay with the chromatogram of 400 µmol L^{-1} ABDA. All samples were illuminated for 30 minutes by a 655 nm laser, filtered and diluted four times prior to the HPLC measurement at 254 nm wavelength.

Therefore, phenolic and quinone derivatives cannot be used, since (i) their oxidized products can be reduced at the electrode surface generating a redox cycle,[2a, 2b] (ii) they react with $^1O_2$ and thus their concentration decreases in time, and (iii) their oxidation products might quench other ROS, rendering the interpretation of the alteration of the photocurrents complicated. Consequently, physical quenchers such as NaN_3 or 1,4-diazabicyclo[2.2.2]octane (DABCO) are often used.[3] They have the advantage that they are not consumed during the quenching of $^1O_2$ and do not generate oxidized species, so the alteration of the photocurrent should solely be dependent on the impact of the quencher on the $^1O_2$ electrochemical reduction.

However, a key prerequisite is that the PS cannot react with the quencher and that the quencher only interacts with $^1O_2$. NaN_3 and DABCO (photo)reduce $F_{64}PcZn$ causing the alteration of the PS's optical bands over the illumination period (Figure S8) and are, thus, unsuitable for the $^1O_2$ quenching in this set-up.[16]

The detection of $^1O_2$ proceeded by using the trap 9,10-anthracenediyl-bis(methylene)dimalonic acid (ABDA), which forms an endoperoxide with $^1O_2$.[17] The decrease of the ABDA concentration upon $^1O_2$ binding (Figure S9 and S10) was quantified via HPLC-DAD measurements. ABDA has a retention time of 8.9 minutes, Figures 4.A and S10. Thus, the red laser illumination for 30 minutes of a solution containing ABDA and $F_{64}PcZn|TiO_2$ (Figure 4.A red) resulted in a 3.3-fold decrease in the ABDA concentration compared to the reference intensity of ABDA (without $F_{64}PcZn|TiO_2$, Figure 4.A black).

The addition of the $^1O_2$ quencher catechol to a solution containing ABDA and $F_{64}PcZn|TiO_2$ (Figure 4.A blue) and the addition of TiO_2 to ABDA alone failed to decrease the ABDA concentration, proving the role of supported $F_{64}PcZn$ (Figure 4.B) in producing $^1O_2$. Catechol efficiently quenched the produced $^1O_2$ due to the slow oxidation rate of $^1O_2$ with ABDA.[17a, 18] The results were consistent with previous observations of polymer encapsulated $F_{64}PcZn|TiO_2$ photoreactivity.[15]

As $^1O_2$ is a strong oxidant (E^0 = 0.65 V vs SHE)[1c], it is expected that it will be reduced at the electrode surface when reductive potentials, such as -0.2 V vs SCE are applied, leading to the formation of ROS $O_2^{\bullet-}$ (eq. 1), H_2O_2 (eq. 2), or H_2O (eq. 3).[1a, 3] The requirement for H^+ ions for the production of H_2O_2 and H_2O suggests enhanced reactivity at lower pH values.

$$^1O_2 + e^- \rightarrow O_2^{\bullet-} \quad (1)$$

$$^1O_2 + 2\ e^- + 2\ H^+ \rightarrow H_2O_2 \quad (2)$$

$$^1O_2 + 4\ e^- + 4\ H^+ \rightarrow 2\ H_2O \quad (3)$$

So, in the next part, the generation of the electrochemical active species $O_2^{\bullet-}$ and H_2O_2, formed upon $^1O_2$ reduction, will be evaluated and it will be investigated if they contribute to the reductive photoresponses.

Identification of $O_2^{\bullet-}$ and H_2O_2

The presence of $O_2^{\bullet-}$ and H_2O_2 was verified using the quenchers SOD and catalase, respectively. In aqueous solution,

$O_2^{\bullet-}$ can easily disproportionate into H_2O_2 and O_2 (eq. 4), enzymatically catalysed by SOD, or non-enzymatically at low pH-levels.[1b, 19] Although, $O_2^{\bullet-}$ is only a mild oxidant, it can be protonated forming the much stronger oxidant $^{\bullet}O_2H$ (pK_a = 4.8) at low pH-levels (eq. 5).[1c, 6] Its reduction also leads to the formation of H_2O_2 (eq. 6).[1a, 1c, 4-5] However, at pH 7 and higher the concentration of $^{\bullet}O_2H$ is negligeable and $O_2^{\bullet-}$ is the dominant specie. Nonetheless, $O_2^{\bullet-}$ is also electrochemically active; depending on the applied potential it can be electrochemically reduced.[4-5, 7b]

$$2\ O_2^{\bullet-} + 2\ H^+ \rightarrow H_2O_2 + O_2 \quad (4)$$

$$O_2^{\bullet-} + H^+ \rightarrow {}^{\bullet}O_2H\ (pK_a = 4.8) \quad (5)$$

$$^{\bullet}O_2H + e^- + H^+ \rightarrow H_2O_2 \quad (6)$$

$$O_2^{\bullet-} + e^- + 2\ H^+ \rightarrow H_2O_2 \quad (7)$$

Thus, when -0.2 V vs SCE is applied, $O_2^{\bullet-}$ will be reduced to H_2O_2 (eq. 7).[1a, 3] Indeed, the $O_2^{\bullet-}$ presence and its contribution to the cathodic photocurrent was confirmed by the addition of SOD which converts $O_2^{\bullet-}$ into O_2 and H_2O_2 (eq. 4),[20] and resulting in a photocurrent decrease by 24% compared to the initial signal in pH 7 (Figure 5.A).

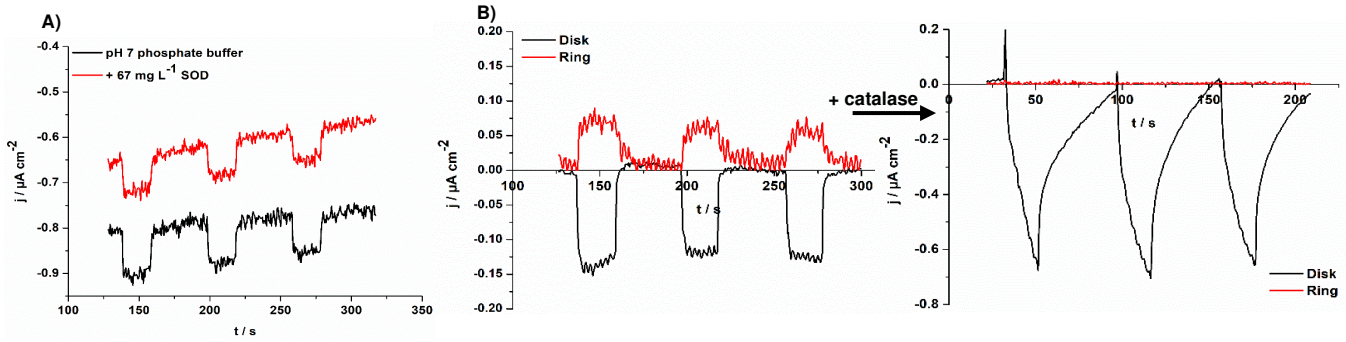

Figure 5. (A) RDE measurements with (red) and without (black) the addition of 67 mg L^{-1} SOD in pH 7 phosphate buffer. The applied potential was -0.2 V vs SCE. (B) RRDE measurements in pH 7 phosphate buffer in the absence (left) and presence (right) of catalase (75 mg L^{-1}). Disk currents are presented in black, ring currents in red. The applied potential of the disk and ring were -0.25 V and 0.65 V vs SCE, respectively. The RDE and disk (RRDE) were coated with $F_{64}PcZn|TiO_2$ and illuminated by a 655 nm laser (switched on and off alternatingly). All measurements were conducted in aerobic conditions.

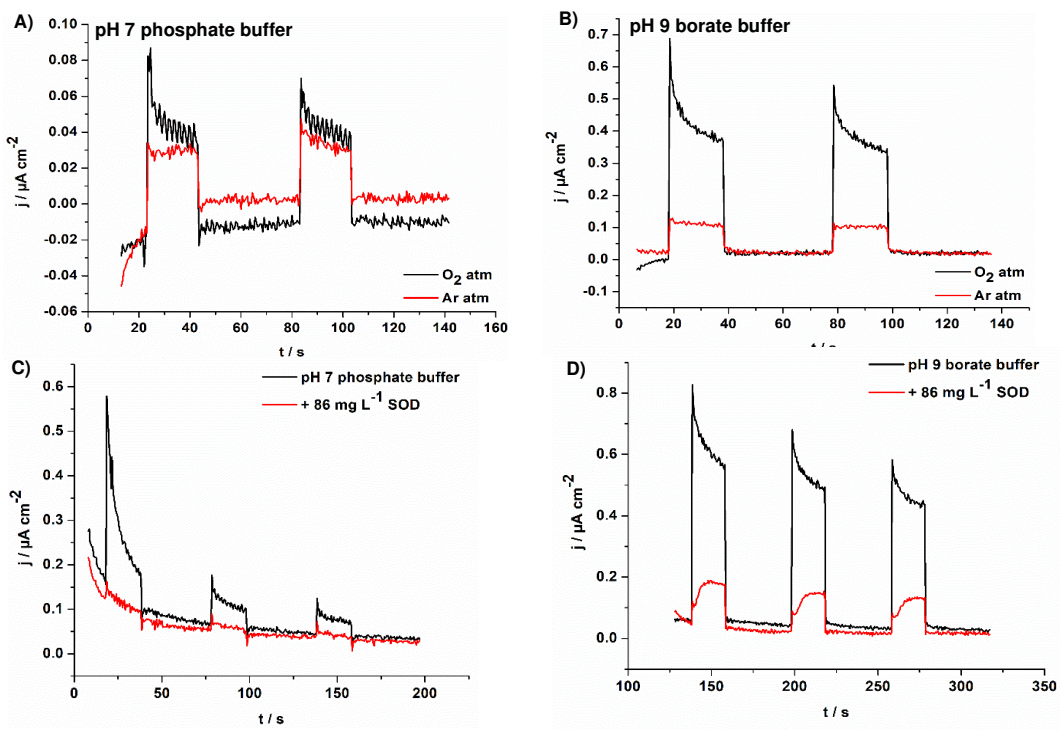

Figure 6. RDE photocurrents measured in O_2 (black) and Ar atmosphere (red) in (A) pH 7 phosphate buffer and (B) pH 9 borate buffer. The effect of 86 mg L^{-1} SOD on the RDE $F_{64}PcZn|TiO_2$ photoactivity measurement in (C) pH 7 phosphate and (D) pH 9 borate buffer in aerobic conditions. The applied potential was 0.2 V vs SCE. The RDE was coated with $F_{64}PcZn|TiO_2$ and illuminated by a 655 nm laser (switched on and off alternatingly).

Clearly, the photocurrents were not significantly influenced by the addition of SOD since $^1O_2$ could also be reduced fast to H_2O_2 and H_2O without the formation of intermediate $O_2^{\bullet-}$, a process which is thus SOD-independent (eq. 2 and 3).[3]. Furthermore, the quenching of $O_2^{\bullet-}$ led to an increased level of O_2 near the electrode surface, thus stimulating $^1O_2$ production, possibly also

explaining why SOD has a only a minor effect on photocurrents intensity.

Most of the H_2O_2, besides being produced chemically via the dismutation of $O_2^{\bullet-}$ at low pH (eq. 4)[1b], is generated electrochemically; a reductive potential, e.g. -0.25 V vs SCE at the glassy carbon (GC) disk electrochemically generates H_2O_2 from $^1O_2$ and $O_2^{\bullet-}$ (eq. 2 and 7). However, at this applied potential, H_2O_2 cannot be reduced (Figure S11). This means that although H_2O_2 is formed, it does not contribute to the PEC observed reductive photoresponses, in contrast to $O_2^{\bullet-}$. So, to detect the produced H_2O_2, a second WE, a Pt ring (WE 2) around the GC disk (WE 1), was thus used for H_2O_2 detection via its oxidation reaction (eq. 8)[5] at 0.65V vs SCE (Figure S12).[3] The rotation of the RRDE ensures that the generated H_2O_2 (lifetime ~ms)[1b, 21] at the $F_{64}PcZn|TiO_2$-coated disk reaches the ring, where it is electrochemically oxidized in the absence or presence of catalase.

$$H_2O_2 \rightarrow O_2 + 2\ e^- + 2\ H^+ \quad (8)$$

$$2\ H_2O_2 \rightarrow 2\ H_2O + O_2 \quad (9)$$

The RRDE measurements in pH 7 (Figure 5.B), revealed ring and disk currents of 54 and -123 nA cm^{-2}, respectively, confirming the ring oxidation of disk-produced H_2O_2. No ring currents were detected in the absence of the disk PS coating (Figure S13). The ring currents decreased significantly upon the addition of catalase, which decomposed H_2O_2 into O_2 and H_2O (eq. 9).[22]

Surprisingly, the disk currents were also affected by the addition of catalase; the photoresponse increased 4.7 times. The increase was likely the result of the catalase-induced formation of O_2, which, in turn, increased the production of $^1O_2$ and thus enhanced its overall reduction level leading to a higher cathodic current at the disk, consistent with the dependency of the cathodic currents on the concentration of O_2 near the electrode surface. However, at pH 9, substantially lower ring currents were detected, likely caused by the instability of H_2O_2 at alkaline pHs[23] and lower disk currents due to lower concentration of H^+ ions needed for the reduction reactions (Figure S14).

In summary, the cathodic currents are found to be dependent on the level of O_2 and are caused by the reduction of $^1O_2$ and $O_2^{\bullet-}$ generating H_2O_2 and H_2O. These reductions are pH-dependent, as they scale inversely with the pH (Figure S18). No electrochemical reduction of the PS occurred at -0.2 V vs SCE, motivating the use of this potential during PEC analysis.

2.4 Anodic photocurrents

The anodic photocurrents were found to increase with the pH even though reductive potentials were applied. This observation requires further explanation in the context of optimization of a detection strategy.[2a] Indeed, the alkalinity of the solution impacts the applied potentials for optimum PEC sensitivity as it shifts the optimum applied reductive potential towards more negative potentials. To reveal the mechanisms behind this oxidative contributions, the anodic responses were studied at a potential of 0.2 V vs SCE at pH 7 and 9 to exclusively exhibit the anodic mechanisms and reveal the influence of ^-OH ions on the photoresponses.

The role of O_2 and $O_2^{\bullet-}$

Firstly, the involvement of O_2 during the anodic photocurrents was evaluated. The purging of the solution with Ar decreased the photoresponse for pH 7 and pH 9 (Figure 6.A and B). At a potential of 0.2 V vs SCE, a limited decrease was noted for pH 7 (Figure 6.A). The photocurrent dropped from 49 nA cm^{-2} in O_2 atmosphere to 37 nA cm^{-2} in an Ar atmosphere. At pH 9, the decrease was more significant (Figure 6.B), 4-fold, in going from O_2 atmosphere to Ar atmosphere.

The addition of SOD to the RDE set-up confirmed the involvement of $O_2^{\bullet-}$, Figure 6.C and D. The generated $O_2^{\bullet-}$ was oxidized to O_2 at the electrode surface, eq. 10 ($E^{0'},ox$ = 0.055 V vs Ag/AgCl)[7b] indicating that the oxidation of $O_2^{\bullet-}$ contributes to the anodic responses. At pH 7 the addition of SOD caused the photocurrent to almost disappear, decreasing from 40 nA cm^{-2} to 6 nA cm^{-2} while at pH 9, a decrease from 470 nA cm^{-2} to 120 nA cm^{-2} was noted.

$$O_2^{\bullet-} \rightarrow O_2 + e^- \quad (10)$$

The formation of $O_2^{\bullet-}$ likely follows two pathways.

Formation of $O_2^{\bullet-}$ via quenching of $^1O_2$ by ^-OH ions (pathway A)

It is known that ^-OH ions quench $^1O_2$ generating $^\bullet OH$ and $O_2^{\bullet-}$ (eq. 11).[24] Thus, as the pH increases (pH 9), the amount of electrochemically reduceable $^1O_2$ decreases, while the generation of $O_2^{\bullet-}$, which is oxidized at 0.2 V vs SCE[7b] (eq. 10) is enhanced, resulting in a higher oxidative contribution to the photocurrent compared to the situation at pH 7 (Figure 6.C and D).

$$^1O_2 + {}^-OH \rightarrow {}^\bullet OH + O_2^{\bullet-} \quad (11)$$

Notably, via this pathway, $^\bullet OH$, one of the strongest oxidizing species (E^0 = 2.33 V vs SHE) is generated.[1c, 4-5] The hydroxyl radical has a lifetime of a few µs, the same order of magnitude as $^1O_2$.[25] Its deprotonated form, $O^{\bullet-}$, is less reactive and it is only present at alkaline pH-levels (pK_a = 11.9).[1a, 4-5] The reactivity of the hydroxyl radicals include $H^\bullet$ abstraction, electron transfer, and electrophilic addition to π systems.[4, 7a, 23a] It degrades organic pollutants[26] and could potentially damage the PS in this PEC system. However, as the local concentration of produced $^\bullet OH$ is high, it can dimerize to form H_2O_2 (eq. 12)[7a, 23a] and thus the concentration of $^\bullet OH$ may be diminished.

$$2\ {}^\bullet OH \rightarrow H_2O_2 \quad (12)$$

The RRDE does not detect H_2O_2 for pH > 9 (Figure S15) since H_2O_2 is unstable at high pH levels.[23] Yet, in the RDE set-up and upon addition of catalase, the photocurrent decreased at pH 9 (Figure 7.B, applied potential was 0.2 V vs SCE). At this potential, H_2O_2 cannot be electrochemically oxidized, since its oxidation requires higher oxidative potentials (Figure S16). So, the oxidation of H_2O_2 does not contribute to the oxidative responses. Rather, the decrease in photocurrent upon the addition of catalase was the result of the generated O_2 upon the decomposition of H_2O_2 by catalase (eq. 9) which seems to enhance the electrochemical reduction of $^1O_2$ at the electrode surface more than the quenching reaction of $^1O_2$ by ^-OH ions as the former pathway is independent on the level of ^-OH ions. Notably, the ^-OH concentration plays an important role in the

generation of H_2O_2 via $^{\bullet}OH$ radicals (eq. 11 and 12) as catalase did not alter the photocurrents at pH 7 indicating that (almost) no H_2O_2 was formed.

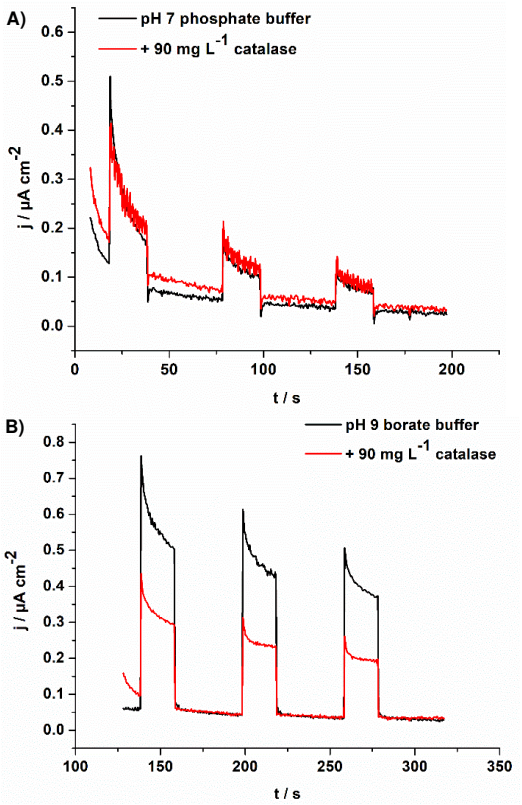

Figure 7. The effect of 90 mg L^{-1} catalase on the photocurrents measured with $F_{64}PcZn|TiO_2$-coated RDE in (A) pH 7 phosphate buffer and (B) pH 9 borate buffer. The applied potential was 0.2 V vs SCE. The RDE surface was illuminated by a 655 nm laser (switch on and off alternatingly). All measurements were conducted in aerobic conditions.

Formation of $O_2^{\bullet-}$ via the reduction of $F_{64}PcZn$ by -OH ions (pathway B)

The high fluorination degree protects PS against oxidation attacks by $^1O_2$, but it enhances the Pc ring susceptibility to reducing agents.[9, 12, 27] The reducibility of the PS was, therefore, studied in the presence of an increasing concentrations of ^-OH ions, which may act as reducing agents for $F_{64}PcZn$, by UV-Vis measurements (Figure 8). The samples were first illuminated for 10 minutes whereafter the UV-vis spectra were recorded. The reduced $[F_{64}PcZn]^{\bullet-}$ form would be visible by the alteration of the optical bands.[12, 16] Indeed, the one-electron redox process is also illustrated by the spectroelectrochemical results shown in Figure S3, which capture the $F_{64}Pc(2\text{-})Zn \leftrightarrow F_{64}Pc(3\text{-})Zn$ process in acetonitrile. The reduction at a Pt mesh electrode is clean, with well-defined isosbestic points. The characteristic Q and selected B bands of $F_{64}Pc(2\text{-})Zn$, 686 and 420 nm, respectively, decrease while the 740, 590 and 468 nm bands corresponding to $F_{64}Pc(3\text{-})Zn$, increase. It is interesting to note that, once the current stopped and the $F_{64}Pc(3\text{-})Zn$ solution is left standing in the absence of light, a spontaneous re-oxidation to $F_{64}Pc(2\text{-})Zn$ occurs, roughly at half-rate of the reduction rate, Figure S3. The electron acceptors might be the solvent, impurities or even traces of oxygen species. The redox process may be important in understanding the electrode processes and their kinetics.

In this case, the addition of KOH, decreased the Q band and increased the intensity of new bands around 588 and 733 nm which corresponded to the reduced $[F_{64}PcZn]^{\bullet-}$ ($F_{64}Pc(3\text{-})Zn$). No photoreduction of the Pc was observed when the KOH was omitted from preparations; only a decrease of the Q band was noted due to the insolubility of the PS in H_2O (Figure S17).

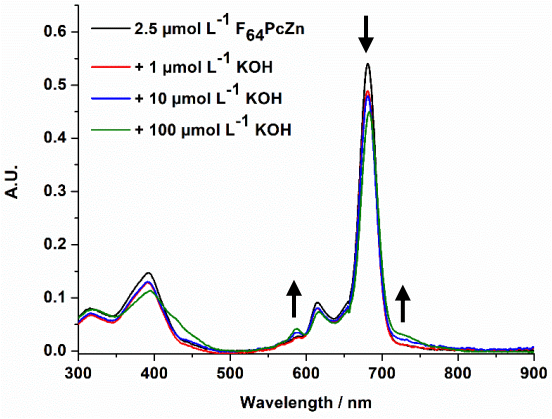

Figure 8. UV-Vis spectra of $F_{64}PcZn$ (2.5 µmol L^{-1}) in MeOH with the addition of 1, 10 and 100 µmol L^{-1} KOH. The spectra were recorded after 10 minutes illumination by a 655 nm laser in aerobic conditions.

The UV-Vis measurements with/without KOH suggest that the PS was reduced by ^-OH ions (eq. 13), proportional with KOH concentration. The ^-OH ions quench $^1O_2$ (pathway A), and reduce the PS (pathway B). The $[F_{64}PcZn]^{\bullet-}$ can be re-oxidized when a potential of 0.2 V vs SCE is applied (eq. 14), or by O_2,[16] or even in the absence of O_2, as shown above. The re-oxidation process, as with the PEC sensor, takes advantage of the $[F_{64}PcZn]^{\bullet-}$ oxidation by O_2 leading to the generation of $O_2^{\bullet-}$ (eq. 15) ,[28] where the latter species can be oxidized at 0.2 V vs SCE (eq. 10). [7b]

$$F_{64}PcZn + {}^-OH \rightarrow {}^{\bullet}OH + [F_{64}PcZn]^{\bullet-} \quad (13)$$
$$[F_{64}PcZn]^{\bullet-} \rightarrow F_{64}PcZn + e^- \quad (14)$$
$$[F_{64}PcZn]^{\bullet-} + O_2 \rightarrow F_{64}PcZn + O_2^{\bullet-} \quad (15)$$

Both A and B pathways contribute to the generation of anodic photoresponses via the oxidation of $O_2^{\bullet-}$ or $[F_{64}PcZn]^{\bullet-}$ which are dependent on the amount of ^-OH ions (Figure S18). Though the reduction of $F_{64}PcZn$ by ^-OH ions might be a minor contributing pathway, its role becomes dominant in the absence of O_2, as the electrochemical oxidation of the reduced species will be the main pathway for the oxidative photocurrents.

3. Conclusion

In this research, the influence of pH and applied potential on the PEC photoresponses was studied via RDE and RRDE measurements. It was observed that the cathodic responses were dependent on the level of H^+ ions while the anodic responses increased with elevating ^-OH ions. $F_{64}PcZn$ deposited on TiO_2 generates $^1O_2$, whose reduction to $O_2^{\bullet-}$ and the reduction of $O_2^{\bullet-}$ to H_2O_2 constitutes key reaction pathway for generating cathodic

photocurrents. The source of anodic photocurrents is complex due to the interplay of ^{-}OH ions on the reduction of $F_{64}PcZn$ and the quenching of $^1O_2$ leading to the generation of $O_2^{\bullet-}$, H_2O_2 and $^{\bullet}OH$. The change of oxidation to reduction of $O_2^{\bullet-}$ plays a crucial role in the shift from anodic to cathodic responses over the studied potential region. The obtained insights in the role of ROS under various experimental conditions are crucial for the selection of optimum experimental parameters for phenol detection as they elaborate the impact of pH-variation on the photoresponses and, thus, the required applied reductive potentials for the $^1O_2$-driven oxidation of phenols. Future work will focus on the interaction of the PS with TiO_2 to study the potential electron injection from $[F_{64}PcZn]^{\bullet-}$ towards the conduction band of TiO_2.

4. Experimental Section

4.1 Materials and methods

Acetonitrile 99.9% (HPLC grade), MeOH, absolute EtOH, acetone and DMF were purchased from commercial sources. Potassium dihydrogen phosphate (KH_2PO_4), borax ($Na_2B_4O_7{\cdot}10H_2O$), boric acid (H_3BO_3) and potassium chloride (KCl) and hydroxide (KOH) were purchased from Sigma-Aldrich, Merck, and Acros Organics, respectively. Buffer solutions were prepared using Milli Q water. $F_{64}PcZn$ (chemical structure in Figure S1) was immobilized on AEROXIDE® TiO_2 P25 (Evonik) matrices with loadings of ~3 wt%, as described previously.[2b] The supported Pc material is abbreviated $F_{64}PcZn|TiO_2$. The quenchers, catalase (from bovine liver), SOD (bovine erythrocytes), NaN_3 and DABCO were purchased from Sigma Aldrich. Catechol (99%) was obtained from J&K Scientific. ABDA was purchased from the Cayman Chemical Company. Graphite SPEs, Ø = 4 mm were purchased from Metrohm DropSens. Al_2O_3 slurries with 1 µm and 0.3 µm particle size (Buehler) and 0.05 µm particle size (SPI Supplies) were used to polish electrodes with a MicroCloth (PSA, 8) acquired from Buehler. A diode laser operating at 655 nm (Roithner Lasertechnik) with a power of 0.24 W cm^{-2} was used as the light source.

4.2 Redox properties of $F_{64}PcZn$

The solution redox properties of $F_{64}Pc(2-)Zn$ are of interest in anticipation of the redox behavior of electrode-supported photosensitizers. CV, DPV and spectroelectrochemical data was obtained in DMF and acetone using a BASi instrument, 0.1 V s^{-1} scan rates and glassy carbon electrode (GCE) and Pt mesh WE. The Ag/AgCl electrode was the reference (RE), 0.1 M Tetrabutylammonium tetrafluoroborate (TBATFB) was the supporting electrolyte. For spectroelectrochemical experiments the counter electrode (CE) was Pt wire.

Additionally, graphite SPEs were used as WE. The RE was a saturated calomel electrode (SCE) and a glassy carbon rod was used as CE. CV (µAutolab III Metrohm Autolab instrument) in 30 mL buffer solutions was used for the determination of redox potentials. The potential was scanned from 1.0 V to -1.0 V vs SCE. The step potential was -0.00244 V and the scan rate was 0.050 V s^{-1}. The components of the buffer solution were 0.02 mol L^{-1} KH_2PO_4 and 0.1 mol L^{-1} KCl. The pH of the buffer was adjusted to 7 by adding dropwise concentrated KOH solution. Before the electrochemical measurements, the cell was purged with Ar gas for 15 minutes to remove dissolved O_2.

For modification of the WE, a stock solution of $F_{64}PcZn$ in EtOH was diluted with Milli Q water to 25 µmol L^{-1}. The final solution contained 27.5 % vol EtOH. This dilution step in water ensured the specific dropcasting on the WE surface. A droplet of 20 µL was then deposited on the WE surface. For blank measurements, 20 µL of a solution containing 27.7 % vol EtOH in Milli Q water was deposited on the WE surface. For the modification of the WE with $F_{64}PcZn|TiO_2$, 3 µL of a 10 mg mL^{-1} aqueous $F_{64}PcZn|TiO_2$ suspension was deposited. As a blank, a TiO_2 modified SPE obtained by dropcasting 3 µL of a 10 mg mL^{-1} TiO_2 aqueous suspension was used. All coatings were dried at room temperature overnight in the absence of light.

4.3 RDE and RRDE measurements of ROS

A Metrohm 628-10 model RDE and a WaveVortex 10 Electrode Rotator from Pine Research RRDE were used. The RDE (Ø = 3 mm) was glassy carbon. The RRDE set-up consists of 2 WEs; the disk electrode GC (Ø = 5 mm) and the ring electrode was Pt. The inner diameter of the Pt ring was 6.5 mm and the outer diameter was 7.5 mm. SCE and glassy carbon rods were used as RE and CE, respectively. The rotation speed of the R(R)DE was 500 rpm.

The RDE and RRDE were polished before each measurement. The RDE was polished with Al_2O_3 slurries of 1, 0.3 and 0.05 µm particle size using a MicroCloth. The disk and ring electrodes of the RRDE were polished with Al_2O_3 slurries of 0.3 and 0.05 µm. The RDE and RRDE were modified with 3 µL or 8.33 µL, respectively, from a 10 mg mL^{-1} aqueous suspension of $F_{64}PcZn|TiO_2$. The droplet on the R(R)DE was dried at 30 °C for 45 minutes.

For the RDE and RRDE measurements, 30 and 80 mL cells were used, respectively. Variable pHs (buffer) were used: 6, 7 and 8 (0.02 mol L^{-1} KH_2PO_4); 9 (0.02 mol L^{-1} H_3BO_3) and 10 (0.02 mol L^{-1} borax). All buffer solutions contained 0.1 mol L^{-1} KCl as supporting electrolyte.

The amperometric measurements were conducted using either a µAutolab III (Metrohm Autolab) instrument for the RDE measurements, or Palmsens 4 BiPot for the RRDE measurements. The RDE surface or disk surface (from RRDE) was illuminated by a 655 nm laser (0.24 W cm^{-2}). The laser was switched on and off alternatingly, respectively 20 seconds on followed by 40 seconds off. The applied potentials were varied between 0.25 V and -0.25 V vs SCE. For the measurements in an Ar atmosphere, the RDE solution was purged for 3 hours with Ar. The photocurrent responses were measured at 0.2 V, -0.15 V and -0.25 V vs SCE at pH 7 and 9. For the identification of $O_2^{\bullet-}$, SOD was used. The applied potential was either 0.2 V (anodic current) or -0.2 V vs SCE (cathodic current). H_2O_2 was identified by the addition of catalase during RRDE measurements. The potential of the ring was 0.65 V vs SCE. The potential of the disk electrode was either 0.25 V or -0.25 V vs SCE. The ring and disk electrode currents were baseline-corrected to improve visibility of the ring currents when plotted together with the disk currents (Figure S2).

4.4 $^1O_2$ detection using ABDA and HPLC

A HPLC-DAD instrument was used to measure the degradation of ABDA by $^1O_2$ as follows. A standard, 100 µmol L^{-1} ABDA was injected to determine first the elution time of this compound. For the oxidation by $^1O_2$, a 2 mL solution containing 0.35 mg mL^{-1} $F_{64}PcZn|TiO_2$ and 400 µmol L^{-1} ABDA in pH 7 phosphate buffer (0.02 mol L^{-1} KH_2PO_4) was made. The solution was illuminated by a 655 nm laser (0.24 W cm^{-2}) for 30 minutes while being magnetically stirred, then filtered (0.45 µm size pore, Chromofil AO-45/25) and diluted 4 times with Milli Q water. The same procedure was applied to a solution containing 0.35 mg mL^{-1} TiO_2 and 400 µmol L^{-1} ABDA. The produced $^1O_2$ was quenched with 50 mmol L^{-1} catechol added to the

$F_{64}PcZn|TiO_2$-ABDA mixture. The same illumination, filtration, and dilution procedures were applied.

The HPLC-DAD experiments were performed with a HPLC system of Shimadzu Prominence LC-20AT coupled to a SPD-M20A DAD with a temperature-controlled flow cell with wavelength range 190-800 nm. A 254 nm wavelength was chosen. The separation was done using a Kinetex C18 column (100 × 4.6 mm id, particle size 2.6 µm) equipped with the appropriate a SecurityGuard cartridge C18, from Phenomenex. The injected volume was 25 µL and the flow rate was kept at 1 mL min^{-1}. Mobile phases consisted of 0.07 % phosphoric acid in ultrapure water (v/v) (solvent A) and acetonitrile/ultrapure water (95/5, v/v) with 0.07 % phosphoric acid (solvent B) to establish the following gradient elution: starting with 2 % solvent B, over the following 13 minutes solvent B linearly increased to 95 %, at 13.1 minutes to 15 minutes the eluent consisted only of solvent B, at 15.1 minutes the eluents again consisted of only 2 % solvent B and was kept for 7 minutes to re-equilibrate the column for the next analysis. All data analysis was performed with the software LabSolutions.

4.5 Stand-alone UV-Vis detection of reduced $F_{64}PcZn$

An Avantes AvaSpec-2048L spectrophotometer and capped (1 cm × 1 cm) 2 mL cuvette was used for the UV-Vis measurements to detect the reduced species of $F_{64}PcZn$. A 655 nm laser beam (0.24 W cm^{-2}) was positioned perpendicular to the optical path and the solution was magnetically stirred. The solution was illuminated for 10 minutes and spectra recorded every 2 minutes.

A 2.5 µmol L^{-1} solution of $F_{64}PcZn$ in MeOH was used. The following compounds were added to this $F_{64}PcZn$ solution: NaN_3 (~10 mmol L^{-1}), DABCO (10 mmol L^{-1}) or KOH. The stock solutions were prepared in MeOH, except for KOH and $F_{64}PcZn$ which were prepared in Milli Q water and EtOH, respectively. The concentration of KOH was varied between 1 µmol L^{-1} and 100 µmol L^{-1} to simulate the effect of increasing alkalinity on $F_{64}PcZn$.

Acknowledgements

FWO is acknowledged for financial support (1S09518N and 1SA5622N) for the work in Belgium. Support by the Center for Functional Materials and DTRA (CB10906) in the USA is gratefully acknowledged. The authors also acknowledge funding from BOF-UAntwerp.

Keywords: Fluorinated Phthalocyanines • Photoelectrochemistry • Reactive Oxygen Species • Rotating (Ring) Disk Electrode • Singlet Oxygen

[1] a) Y. Nosaka, A. Y. Nosaka, *Chem Rev* **2017**, *117*, 11302-11336; b) K. Das, A. Roychoudhury, *Front Environ Sci* **2014**, *2*, 1-13; c) K. Krumova, G. Cosa, in *Singlet Oxygen: Applications in Biosciences and Nanosciences, Volume 1, Vol. 1* (Eds.: S. Nonell, C. Flors), The Royal Society of Chemistry, Cambridge, UK, **2016**, pp. 1-21.

[2] a) L. Neven, S. T. Shanmugam, V. Rahemi, S. Trashin, N. Sleegers, E. N. Carrion, S. M. Gorun, K. De Wael, *Anal Chem* **2019**, *91*, 9962-9969; b) S. Trashin, V. Rahemi, K. Ramji, L. Neven, S. M. Gorun, K. De Wael, *Nat Commun* **2017**, *8*; c) M. M. Rahman, M. M. Alam, A. M. Asiri, *Nanoscale Adv* **2019**, *1*, 696-705.

[3] N. Kornienko, J. Z. Zhang, K. P. Sokol, S. Lamaison, A. Fantuzzi, R. van Grondelle, A. W. Rutherford, E. Reisner, *J Am Chem Soc* **2018**, *140*, 17923-17931.

[4] F. Collin, *Int J Mol Sci* **2019**, *20*, 2407.

[5] W. H. Koppenol, D. M. Stanbury, P. L. Bounds, *Free Radic Biol Med* **2010**, *49*, 317-322.

[6] P. Pospisil, A. Prasad, M. Rac, *Biomolecules* **2019**, *9*, 1-21.

[7] a) A. Medel, J. Trevino-Resendez, E. Brillas, Y. Meas, I. Sires, *Electrochim Acta* **2020**, *331*; b) X. C. Zhao, M. N. Zhang, Y. T. Long, Z. F. Ding, *Can J Chem* **2010**, *88*, 569-576; c) Y. Zheng, W. Chen, X.-Q. Zuo, J. Cai, Y.-X. Chen, *Electrochem Commun* **2016**, *73*, 38-41; d) E. Sitta, A. M. Gómez-Marín, A. Aldaz, J. M. Feliu, *Electrochem Commun* **2013**, *33*, 39-42.

[8] a) Y. F. Zhang, M. H. Dai, Z. H. Yuan, *Anal Methods* **2018**, *10*, 4625-4638; b) C. E. Diaz-Uribe, M. C. Daza, F. Martínez, E. A. Páez-Mozo, C. L. B. Guedes, E. Di Mauro, *J Photochem Photobiol A: Chem* **2010**, *215*, 172-178; c) H. Zhu, Z. Jia, M. A. Trush, Y. R. Li, *React Oxyg Species (Apex)* **2016**, *1*, 216-227; d) V. G. Grivennikova, A. V. Kareyeva, A. D. Vinogradov, *Redox Biol* **2018**, *17*, 192-199; e) H. S. Choi, J. W. Kim, Y. N. Cha, C. Kim, *J Immunoassay Immunochem* **2006**, *27*, 31-44.

[9] A. Loas, R. Gerdes, Y. Y. Zhang, S. M. Gorun, *Dalton Trans* **2011**, *40*, 5162-5165.

[10] M.-S. Liao, J. D. Watts, S. M. Gorun, S. Scheiner, M.-J. Huang, *J Theor Comput Chem* **2008**, *07*, 541-563.

[11] H. Z. Zhang, C. H. Lin, L. Sepunaru, C. Batchelor-McAuley, R. G. Compton, *J Electroanal Chem* **2017**, *799*, 53-60.

[12] S. P. Keizer, J. Mack, B. A. Bench, S. M. Gorun, M. J. Stillman, *J Am Chem Soc* **2003**, *125*, 7067-7085.

[13] M. de Jong, A. Florea, A.-M. d. Vries, A. L. N. van Nuijs, A. Covaci, F. Van Durme, J. C. Martins, N. Samyn, K. De Wael, *Anal Chem* **2018**, *90*, 5290-5297.

[14] R. Minnes, H. Weitman, H. J. Lee, S. M. Gorun, B. Ehrenberg, *Photochem Photobiol* **2006**, *82*, 593-599.

[15] a) A. Azeez, L. Polio, J. E. Hanson, S. M. Gorun, *ACS Appl Polym* **2019**, *1*, 1514-1523; b) S. M. Gorun, J. Sullivan, R. Karpagavalli, Porter Scientific Inc, **2016**.

[16] H. Moons, A. Loas, S. M. Gorun, S. Van Doorslaer, *Dalton Trans* **2014**, *43*, 14942-14948.

[17] a) T. Entradas, S. Waldron, M. Volk, *J Photochem Photobiol B: Biol* **2020**, *204*, 111787; b) X. Q. Shen, L. Li, H. Wu, S. Q. Yao, Q. H. Xu, *Nanoscale* **2011**, *3*, 5140-5146.

[18] N. A. Garcia, *J Photochem Photobiol B: Biol* **1994**, *22*, 185-196.

[19] R. G. Petasne, R. G. Zika, *Nature* **1987**, *325*, 516-518.

[20] J. M. McCord, I. Fridovic., *J Biol Chem* **1969**, *244*, 6049-6055.

[21] F. J. Schmitt, G. Renger, T. Friedrich, V. D. Kreslavski, S. K. Zharmukhamedov, D. A. Los, V. V. Kuznetsov, S. I. Allakhverdiev, *BBA-Bioenergetics* **2014**, *1837*, 835-848.

[22] M. Alfonso-Prieto, X. Biarnes, P. Vidossich, C. Rovira, *J Am Chem Soc* **2009**, *131*, 11751-11761.

[23] a) O. Legrini, E. Oliveros, A. M. Braun, *Chem Rev* **1993**, *93*, 671-698; b) O. Spalek, J. Balej, I. Paseka, *J Chem Soc Faraday Trans* **1982**, *78*, 2349-2359.

[24] A. E. H. Machado, A. J. Gomes, C. M. F. Campos, M. G. H. Terrones, D. S. Perez, R. Ruggiero, A. Castellan, *J Photochem Photobiol A: Chem* **1997**, *110*, 99-106.

[25] Y. Nosaka, T. Daimon, A. Y. Nosaka, Y. Murakami, *Phys Chem Chem Phys* **2004**, *6*, 2917-2918.

[26] M. Cheng, G. Zeng, D. Huang, C. Lai, P. Xu, C. Zhang, Y. Liu, *Chem Eng J* **2016**, *284*, 582-598.

[27] a) H. Moons, H. H. Patel, S. M. Gorun, S. V. Doorslaer, *Z Phys Chem* **2017**, *231*, 887-903; b) E. N. Carrión, A. Loas, H. H. Patel, M. Pelmuş, K. Ramji, S. M. Gorun, *J Porphyr Phthalocyanines* **2018**, *22*, 371-397.

[28] a) C. Li, M. Z. Hoffman, *J Phys Chem A* **2000**, *104*, 5998-6002; b) M. S. Baptista, J. Cadet, P. Di Mascio, A. A. Ghogare, A. Greer, M. R. Hamblin, C. Lorente, S. C. Nunez, M. S. Ribeiro, A. H. Thomas, M. Vignoni, T. M. Yoshimura, *Photochem Photobiol* **2017**, *93*, 912-919.

Entry for the Table of Contents

Insert graphic for Table of Contents here.

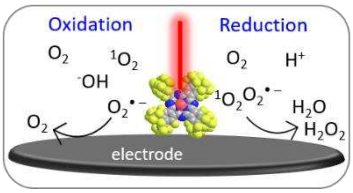

Unravelling the role of reactive oxygen species formed upon illumination of a photosensitizer type II, $F_{64}PcZn|TiO_2$, during photoelectrochemical sensing. The species were identified using rotating (ring) disk electrode, UV-Vis and HPLC-DAD measurements. Their generation and corresponding photocurrents magnitude is highly dependent on the pH and applied potential.